



# Seismic behavior assessment of RC buildings controlled by passive and active techniques

## Pasif ve aktif tekniklerle kontrol edilen betonarme binaların sismik davranışlarının değerlendirilmesi

Mustafa Ergün<sup>1,\*</sup> , Mehmet Uyar<sup>2</sup> 

<sup>1</sup> Bayburt University, Department of Civil Engineering, 69000, Bayburt, Türkiye

<sup>2</sup> Bayburt University, Department of Mechanical Engineering, 69000, Bayburt, Türkiye

### Abstract

In this paper, a numerical study was carried out on the effectiveness of the active earthquake control method in improving the earthquake response of RC buildings. High damping rubber bearing design was made according to the criteria of the Uniform Building Code. Three different types of isolators were obtained geometrically. Passive earthquake control of the building was provided by placing these isolators under the columns. For active earthquake control of the building, controller design was realized by integrating it into the FE transient analysis in ANSYS. The active earthquake control design was studied using a force-based and displacement-based controller with acceleration and displacement feedback. The linear dynamic earthquake analysis in the time history of all three states of the building (un-controlled, passive, and active-controlled) was made using the acceleration record of the Seferihisar (İzmir) earthquake. When the results are examined, it is seen that the active earthquake control method provides almost all of the positive behavior expected from the passive earthquake control method. In addition, it eliminates some of the disadvantages of the passive earthquake control method.

**Keywords:** Reinforced concrete building, High damping rubber bearing, Passive earthquake control, Active earthquake control, Actuator type, Actuator location

### 1 Introduction

Earthquakes occur as due to compression, friction, and sliding movements that occur along the boundary lines of the plates that make up the Earth's crust (Figure 1a). According to the Global Earthquake Risk Map, it can be said that the earthquakes occurring on the Earth are concentrated in a specific region. Generally, earthquakes occur at the borders of the plates that make up the Earth's crust (Figure 1b). This supports the Elastic Rebound Theory, which argues that the energy accumulated in the Earth's crust of the earthquake is released by fault action. The regions where earthquakes are observed intensely are gathered in three main belts on Earth; Pacific Seismic Belt, Alpine-Himalayan Seismic Belt, and Atlantic Seismic Belt.

### Öz

Bu makalede, betonarme binaların deprem davranışını iyileştirmede pasif deprem kontrol yöntemine bir alternatif olarak aktif deprem kontrol yönteminin etkinliği üzerine sayısal bir çalışma gerçekleştirilmiştir. Binanın pasif kontrolü için gerekli olan yüksek sönümlü kauçuk izolatörlerin tasarımı Uniform Bina Yönetmeliği kriterlerine göre yapılmıştır. Geometrik olarak üç farklı tip izolatör elde edilmiştir. Bu izolatörler kolonların altına yerleştirilerek binanın pasif deprem kontrolü sağlanmıştır. Bina aktif kontrolü için kullanılan kontrolör tasarımı, ANSYS'te sonlu eleman tabanlı zaman tanım alanında analizlere entegre edilerek gerçekleştirilmiştir. Aktif deprem kontrol tasarımı, ivme ve yer değiştirme geri beslemeli kuvvet tabanlı ve yer değiştirme tabanlı bir kontrolör kullanılarak incelenmiştir. Yapının her üç durumunun (kontrolsüz, pasif kontrollü ve aktif kontrollü) zaman tanım alanında doğrusal deprem analizi, Seferihisar (İzmir) depreminin ivme kaydı kullanılarak yapılmıştır. Sonuçlar incelendiğinde aktif deprem kontrol yönteminin pasif deprem kontrol yönteminden beklenen olumlu davranışların tamamına yakınına sağladığı ve bununla birlikte pasif deprem kontrol yönteminin bazı dezavantajlarını da ortadan kaldırdığı görülmektedir.

**Anahtar Kelimeler:** Betonarme bina, Yüksek sönümlü kauçuk izolatör, Pasif deprem kontrolü, Aktif deprem kontrolü, Aktüatör tipi, Aktüatör konumu

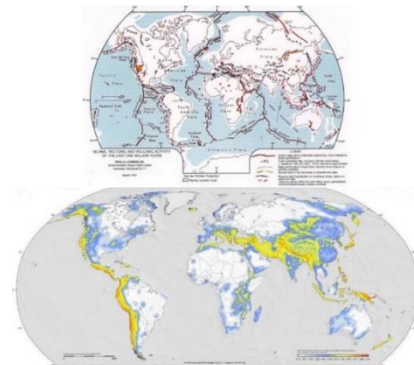


**Figure 1.** Plate tectonics map [1], Global earthquake risk map [2]

\* Corresponding author, e-mail: mustafaergun@bayburt.edu.tr (M. Ergün)

Geliş / Recieved: 22.06.2023 Kabul / Accepted: 09.10.2023 Yayınlanma / Published: 15.01.2024

doi: 10.28948/ngumuh.1318649

The seismotectonic structure of Turkey, located on the Alpine-Himalayan seismic belt, one of the most active seismic belts in the world, is formed mainly by the movements of the African-Arabian plates. Due to the spreading of the mid-Atlantic ridge toward both sides, the African-Arabian plates are moving towards the north-northeast. In addition, the northward movement of the Arabian plate due to the seafloor spreading along the Red Sea forces the Anatolian plate to subduct under the Eurasian plate (Figure 2).

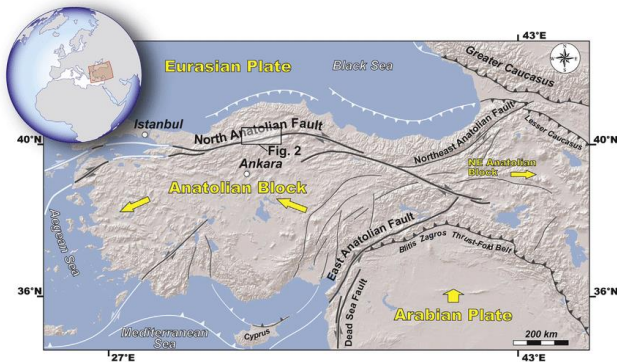


**Figure 2.** Position and directions of motion of the Anatolian plate [3]

Such a movement of the Anatolian plate creates numerous faults and, as a result, earthquakes. As a result of this migration, two major faults developed: the North Anatolian Fault and the East Anatolian Fault. Compression movement has occurred in these faults for millions of years, Turkey's primary cause of earthquakes. In the Greece-Aegean geography, the Earth's crust tries to stop the Anatolian plate from moving westward. This obstacle forces Western Anatolia to expand, resulting in depressions and elevation zones known as graben and horst. The fault that developed due to this migration is known as the West Anatolian Fault.

Turkey's lands, population, and industrial facilities are in active earthquake zones. Since the establishment of the Republic of Turkey, severe earthquakes have occurred in these lands over the years, and as a result, many people have lost their lives. In addition, many buildings have been destroyed or severely damaged. As a result, it is of great importance for Turkey, which is an earthquake country, to take some precautions against earthquakes that cause the death of hundreds of people and the destruction of thousands of buildings on average every year.

Many studies have been carried out in earthquake engineering and earthquake-resistant structure design to minimize these adverse effects of earthquakes on all living creatures for years. One of the most critical developments in this field is the seismic isolation systems that protect the buildings against the earthquake's devastating effects by reducing the earthquake forces transferred to the building. The load-bearing capacity, stiffness, ductility, stability, and inelastic deformation of a building can be increased by modifications to the structural system (conventional methods). Developed as an alternative to these traditional methods, seismic isolation systems are applied to minimize

the destructive effects of earthquakes by increasing the energy consumption capacity and period of buildings [4,5].

The seismic isolation system, based on the idea of separating the foundation and ground, is applied to the structure with various types of isolators, extending the period of the structure, reducing the incoming earthquake load, and reducing the relative story drift. For this reason, the seismic isolation system has been widely used for years worldwide, both in designing new buildings against earthquakes and increasing the earthquake performance of existing buildings [6-44].

In addition to all these positive aspects of the seismic isolation system, some disadvantages should be considered. For example, (i) If the building is exposed to a more giant earthquake than the design earthquake, there may be permanent damage to the isolators and rupture. (ii) The costs of seismic isolators are pretty high. In addition, the need for an extra basement floor, deeper excavation of the foundation, and the surrounding of the foundation with retaining walls so that the structure can make displacement increase the cost of insulated buildings. (iii) Since seismic isolation systems prolong the periods of the structures, they are not suitable for buildings resting on soft soils. The seismic isolation system for buildings resting on soft ground will increase the earthquake load on the structure. In addition, considering the hammer effect that may occur during an earthquake in adjacent structures, seismic isolation system can cause significant damage to such buildings. (iv) Isolators cannot be partially applied to a building. It is applied to the building as an isolation system, such as an isolator group. Therefore, implementation efficiently is complex and often requires highly skilled laborers and engineers. (v) The seismic isolation system causes large displacements in the building. If the displacement values exceed the regulations' limits, risky situations may occur for the building.

One of the most important aims of this study is to use an alternative method that will both include the advantages of the seismic isolation system and eliminate the disadvantages mentioned above to enhance the seismic performance of RC buildings. For this purpose, an active earthquake control (AEC) system has been applied to the building.

Vibration control is one of the most effective methods for damping vibrations caused by earthquakes to protect people's lives and ensure safety. ATMD achieves the AEC by creating a vibration response in the opposite direction to the movement of the building through the control force created with the actuator to dampen seismic vibrations. Many studies have been carried out on active and passive vibration control in buildings to minimize seismic vibrations caused by earthquakes. Umutlu et al. [45] designed a robust adaptive controller to suppress the undesired vibrations from an earthquake on multistory buildings. Soleymani et al. [46] proposed a new robust control approach, a two-loop sliding mode controller with a dynamic state predictor to suppress the vibrations of a high-rise building. Collette and Chesné [47] proposed a hybrid mass damper (HMD) design consisting of passive and active elements. To reduce the vibration amplitudes of a multi-degrees-of-freedom structure, the power consumption and vibration reduction

amounts are presented in comparison with the direct speed feedback controller and the classical control method. Mamat et al. [48] compared the effectiveness of sliding mode control and fuzzy logic controller applied the structural vibration control. Guclu and Yazici [49] designed the fuzzy logic and PD controllers with an ATMD to reduce the effect of earthquake vibrations in a multi-degree-of-freedom building. Also, PID and sliding mode controller (SMC) are separately improved to simulate the ground motion of the Marmara earthquake for a multi-degree-of-freedom structural system. Xu et al. [50] studied an ATMD-based vibration control that considers the actuator saturation to reduce vibrations generated against seismic excitations in adjacent buildings. Heidari et al. [51] simulated seismically excited structures to compare the performance of a hybrid active control method consisting of PID and LQR control algorithms. Karami et al. [52] designed a new semi-ATMD controller that combines damage detection and semi-active control approach due to structural frequency variations.

When all these studies are examined, it can be seen that the AEC method with an actuator gives significant results in damping earthquake vibrations in buildings. In addition to the results from these studies, this study demonstrates that AEC is a powerful alternative to passive earthquake control (PEC) in improving the seismic performance of RC buildings, with a case study on an actual RC building model. Active vibration control studies in the literature are generally based on frame systems. Studies on real 3D building models are limited. In this study, a real 3D building model was used. Besides, some problematic situations of PEC mentioned above have been eliminated by AEC.

This study has been completed by completing the following basic steps: i) Linear dynamic earthquake analyses in the time history of the uncontrolled building were performed using the acceleration record of the Seferihisar (İzmir) earthquake. ii) The design of the high-damping rubber bearing (HDRB) was made by the Uniform Building Code (UBC-97) [53] and Turkey Earthquake Building Code (TEBC-2018) [54] criteria. iii) Linear dynamic earthquake analyses in the time history of the passive earthquake-controlled building were performed using the acceleration record of the Seferihisar (İzmir) earthquake. iv) The active force-based and displacement-based control designs were proposed with acceleration and displacement feedback. The

control design was adopted for the proportional-integral-derivative (PID) control system for the building excited to the earthquake. Linear dynamic earthquake analyses in the time history of the active earthquake-controlled building were performed using the acceleration record of the Seferihisar (İzmir) earthquake. v) As a result of the analysis made for all three cases, the maximum displacement, velocity, and acceleration values along the height of the building were obtained as the earthquake behavior parameters of the structure. Besides, displacement, velocity, and acceleration values read in time history from selected nodes were taken. vi) By comparing the obtained results, it has been revealed that AEC can be a powerful alternative to PEC in improving the seismic performance of RC buildings. It has also been shown that AEC can eliminate some of the known disadvantages of PEC.

### 1.1 Model description

The studies in this paper were carried out on an RC building. The skeleton system of the building consists of a traditional frame system. The building, whose plan, longitudinal section, and 3D views are given in Figure 3, has three floors, each 3 m high, and has two spans of 5 m in the x and y directions.

The vertical carrier system of the building consists of only columns. Reinforced concrete shear walls were not used. The dimensions of the columns are the same throughout the height of the building, and the value is 40/40. There are 36 beams in total in the building. The dimensions of the beams are 25/50. Except for the attic beams, all have brick walls 13 cm thick. The value of the constant load transferred from the walls to the beams is 0.25 t/m<sup>2</sup>. The building consists of 12 slabs in total. The thickness of the slabs is 15 cm. There are dead and live loads on all slabs with values of 0.15 t/m<sup>2</sup> and 0.2 t/m<sup>2</sup>, respectively. The same type of material was used for all the structural elements; C25/B420C. The effect of the rebar on the structural behavior was neglected; only its weight was considered in the analyses. C25 concrete class, whose characteristic features are shown in Table 1, has been selected considering the code criteria. Because according to TEBC-2018, there is a condition that concrete cannot be used in a class lower than C25 in the construction of RC buildings.

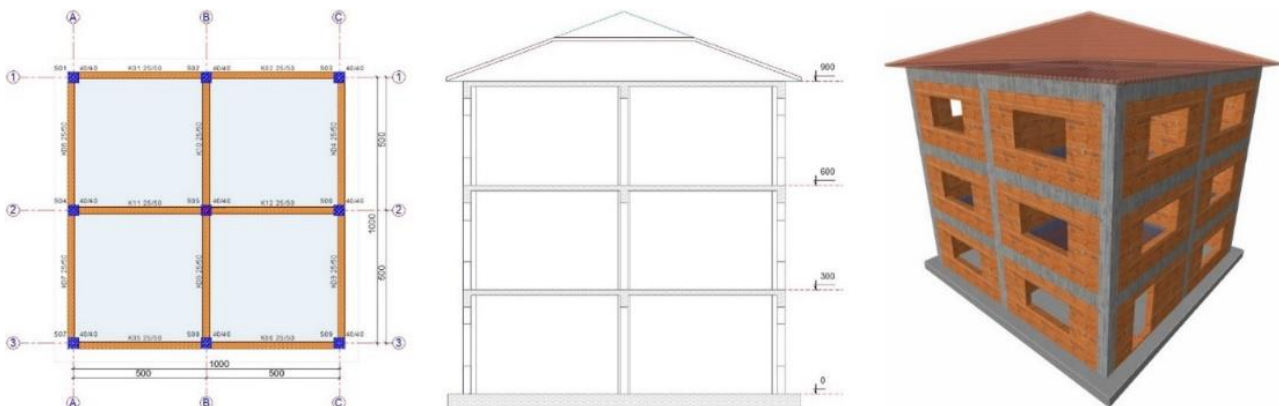


Figure 3. Geometric characteristics of building

**Table 1.** C25 concrete

Characteristic cylinder compressive strength (MPa)	25
Mean tensile strength (MPa)	1.75
Factor of safety	1.5
Elastic modulus (MPa)	30250
Shear modulus (MPa)	12604.167
Poisson's ratio	0.2
Density (N/mm <sup>3</sup> )	0.000025
Coefficient of linear thermal expansion	10 <sup>-5</sup>

Seferihisar district of İzmir province was chosen as the region where the building will be constructed. The reason for choosing this region is that one of the last devastating earthquakes in Turkey occurred in this region in 2020. As a result, including a region with seismic activity in the analysis produced more realistic results. In the section that follows, specific details regarding the area's seismic activity are provided.

### 1.2 Seismicity of the region

Under the Western Anatolian Opening Regime, Izmir province is positioned at the western end of the Gediz Graben system. E-W trending normal faults are located near the west end of the Gediz Graben, as seen in the active fault map of Turkey created by the General Directorate of Mineral Research and Exploration (MTA) in 2011. In contrast, NE-SW and NW-SE faults are concentrated around Izmir (Figure 4). Also, the active faults of Gumudur, Yeni Foca, Seferihisar, Guzelhisar, Gulbahce, Kiraz, Menemen, Tuzla, Izmir, and Mordagan may be a source of earthquake activity in the region.



**Figure 4.** Distribution of active faults in the region [55]

Since 1900, 695  $M \geq 4.0$  earthquakes, the largest of which is 6.8, have occurred in the region. In addition, there are 332 historical earthquake records for the region before 1900 (Figure 5).

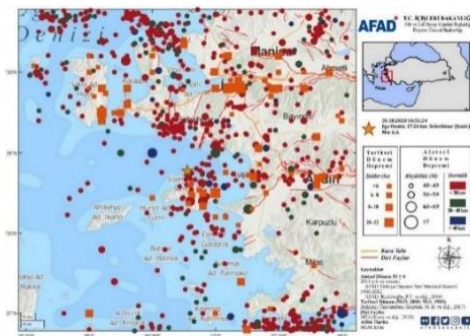


**Figure 5.** Historical and instrumental period earthquake activity of the region [56].

According to the previous Turkey Regional Earthquake Map, İzmir is in the earthquake zone I category (Figure 6a). The new map depicts peak ground acceleration values depending on the distances to the faults rather than dividing the country into earthquake zones with specific boundaries (Figure 6b). It was published in March 2018 with more detailed seismic hazard analysis, including next-generation mathematical algorithms, instrumental and historical earthquake catalogs, and the most recent earthquake source parameters. In the Turkey Earthquake Hazard Map, the maximum acceleration value of İzmir province PGA 475(year) varies between 0.3-0.5g. This parameter shows that the region's earthquake risk is relatively high, and the earthquake phenomenon must be considered in designing new buildings to be built here.

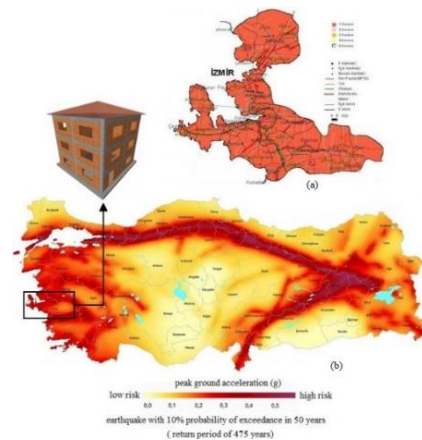


**Figure 6.** Regional earthquake map (a) and Turkey's new earthquake hazard map (b) [56]

## 2 Studies

Various numerical analyses were carried out in the studies section of the paper following the previously specified purpose and objectives. This section was split into three main subheadings; i) studies on dynamic earthquake analysis of RC buildings fixed to the ground (Un-controlled), ii) studies on the dynamic earthquake analysis of RC buildings with seismic isolation (passive earthquake control) at foundation level, iii) studies on dynamic earthquake analysis of reinforced concrete building under the influence of active earthquake control method. All building analyses considered in this study were carried out simultaneously using SAP2000 [57] and ANSYS [58] package programs. The studies carried out under these sub-headings are explained in detail in the following sections.

### 2.1 Dynamic earthquake analysis of un-controlled RC building

The dynamic earthquake analysis of the building considered in this section was made using ANSYS. The building was modeled in three dimensions, adhering to the geometric and material properties in the previous section and the finite element method (FEM) criteria. Shell components represented slabs in the FEM, while frame elements represented beams and columns. The FEM had 372

connection points, 300 shell elements, and 153 frame elements. The model has 10 m, 10 m, and 9 m dimensions in the X, Y, and Z axes, respectively (Figure 7).

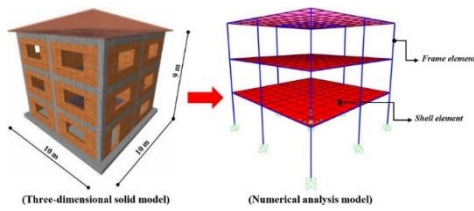


**Figure 7.** Three-dimensional solid and numerical models of the un-controlled RC building

For the frame and shell elements on the numerical analysis model, BEAM188 and SHELL181 element types from the ANSYS library were preferred, respectively. The geometric properties of both elements are given in Figure 8.

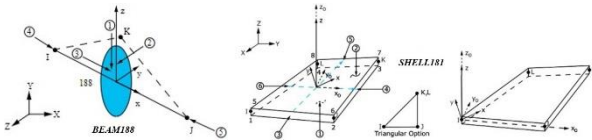


**Figure 8.** Geometric properties of BEAM188 and SHELL181 elements, respectively [58]

BEAM188 is an element used to analyze particularly thin and, in some cases, reasonably stubby/thick frame elements. The numerical model for this element is based on the Timoshenko beam theory, which considers shear-deformation effects. It contains six degrees of freedom at each node, including rotations around the x, y, and z axes and translations in the x, y, and z directions—this element best serves linear, large rotational, and nonlinear strain applications [58].

SHELL181 is an element type that can study moderately thick shell elements. It is a four-node element with six degrees of freedom at each node, including rotations around the x, y, and z axes and translations in the x, y, and z directions. This element best serves linear, large rotational, and nonlinear strain applications [58].

The seismic sensitivity evaluation of the building considered in this study was evaluated under the influence of the Seferihisar (Izmir) earthquake. It happened offshore in the Aegean Sea on October 30, 2020, at 14:51 Turkish time, between Samos Island's north and Doganbey-Izmir. The earthquake's moment magnitude was recorded at 6.6, and the focal depth is around 15 km. The closest community, Doanbey Payamli village in Izmir's Seferihisar district, is 23.38 kilometers from the earthquake's epicenter. The precise duration of the quake was determined as 15.68 seconds. A large area encompassing the Aegean and Marmara areas and the province and districts of Izmir felt the effects of the earthquake. According to the intensity map produced using the Earthquake Preliminary Damage Estimation System (AFAD-RED) [56], the earthquake's intensity in the settlement closest to the earthquake's epicenter, within Turkey's borders, was calculated as MMI VII.

The characteristics of the Seferihisar (Izmir) earthquake are given in Table 2. The graphs of the acceleration, velocity, and displacement records for both horizontal components of the earthquake are shown in Figures 9-11, respectively. The earthquake records were taken from the Aydın (Kusadasi) station (PGA: 18.279 cm/s<sup>2</sup>, PGV: 7.845 cm/s, PGD: 2.257 cm).

**Table 2.** The characteristics of the Seferihisar (Izmir) earthquake [56].

PGA (cm/s <sup>2</sup> )	179.31 (TK.0905 NS, Rept:49.38 km)	
PGV (cm/s)	22.53 (TK.3519 NS, Rept:73.08 km)	
PGD (cm)	5.16 (TK.3518 UD, Rept:72.48 km)	

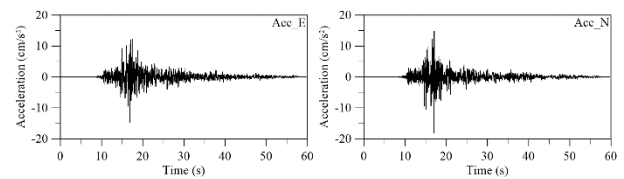


**Figure 9.** Acceleration records of the Seferihisar (Izmir) earthquake [56]

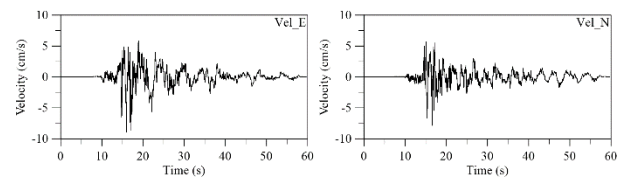


**Figure 10.** Velocity records of the Seferihisar (Izmir) earthquake [56]

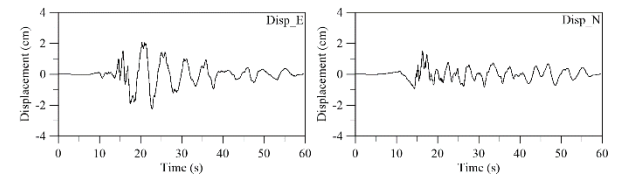


**Figure 11.** Displacement records of the Seferihisar (Izmir) earthquake [56]

Free vibration analysis was made to define the modal manner of the building to be necessary before starting the earthquake analysis in the time history of the building. The adequate number of vibration modes to be considered in the free vibration analysis should be established according to the total of the effective modal masses of the base shear force calculated for each mode in the (X) and (Y) directions. This value cannot be less than 95% of the building's overall mass. [54]. As a result of the analysis, this criterion was met for the first ten modes. Total mass participation rates in the building's X and Y directions were calculated to be 99% for each (Figure 12). The first three mode shapes and dynamic properties of the structure are also given, respectively, in Figure 13 and Table 3.

**Table 3.** Comparison of dynamic characteristics of the building according to different package programs.

Packaged Software	Mode I			Mode II			Mode III		
	Frequency (Hz)	Period (s)	Angular Freq. (rad/s)	Frequency (Hz)	Period (s)	Angular Freq. (rad/s)	Frequency (Hz)	Period (s)	Angular Freq. (rad/s)
ANSYS	2.427	0.412	15.249	2.427	0.412	15.249	3.052	0.328	19.176
SAP2000	3.033	0.330	19.057	3.033	0.330	19.057	3.876	0.258	24.354
ideCAD	2.328	0.430	14.627	2.328	0.430	14.627	2.800	0.357	17.593

Dynamic characteristics give us essential information about whether the numerical model of any structure is correct. In this study, the dynamic characteristics of the building were calculated numerically. No model validation was performed with an experimental study such as operational modal analysis. For this reason, free vibration analysis of the building was performed using three different software package programs. When the data given in Table 3 are examined, it is seen that the results are consistent and very close to each other. This shows that the numerical model of the building is correct.

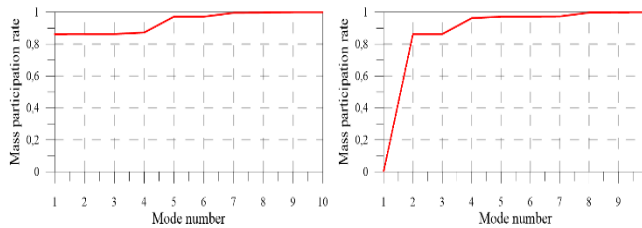


**Figure 12.** Total mass participation ratios in the X and Y directions, respectively

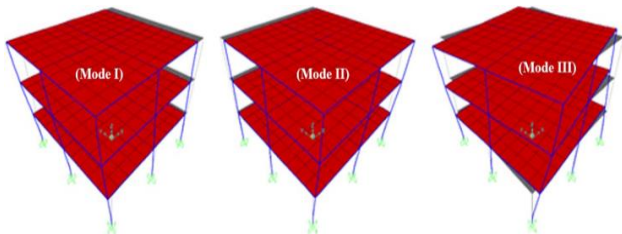


**Figure 13.** The first three mod shapes of the building

It was observed that the structure's concrete and rebar materials remained in the liner-elastic region as a result of the preliminary dynamic analysis. In addition, the second-order effects that occurred were also within the allowable limit values. When the structural behavior parameters obtained as a result of both linear and nonlinear analyzes were examined, it was seen that there were no meaningful differences between the results. In addition to all these reasons, linear analysis was chosen as the dynamic earthquake analysis method to save time and labor.

Linear dynamic earthquake analyses in the time history of the building were performed using the Acc\_E record of the Seferihisar (İzmir) earthquake with the help of the ANSYS program. The reason for using this earthquake record is that the PGA value of this record is greater than one of the Acc\_N records (Figure 9). The five-second period with the peak acceleration values was used to shorten the analysis time. The earthquake effect was applied in the X-direction, which is the dominant vibration mode direction of

the structure. As a result of the analysis, the maximum displacement, velocity, and acceleration values along the height of the structure were obtained as the earthquake behavior parameters of the building. Besides, displacement, velocity, and acceleration values read in time history from A, B, and C nodes were taken. These results are shown in Figures 14-17.

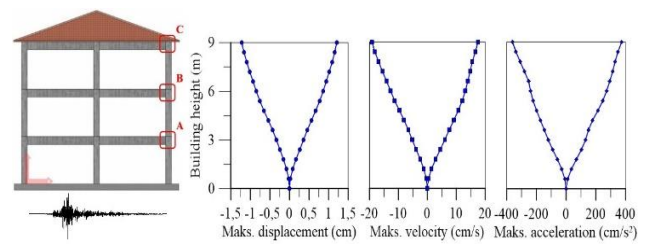


**Figure 14.** Distribution of maximum displacement, velocity and acceleration values along the height of the building

Figure 14 indicates the maximum amplitudes of displacement, velocity, and acceleration responses at each node along the stories in the building. For uncontrolled situations, maximum displacement, velocity, and acceleration values are approximately  $\pm 1.5$  cm,  $\pm 20$  cm/s, and  $\pm 400$  cm/s<sup>2</sup>, respectively. As seen in Figure 14, vibration amplitudes tend to increase almost linearly along the height of the building. This situation causes the relative structural behavior to be large and the internal forces to increase accordingly.

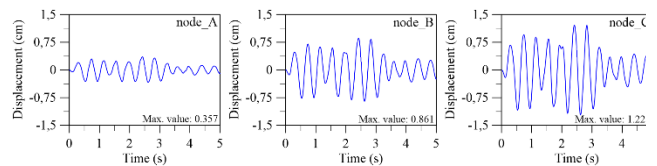


**Figure 15.** Time history displacements at nodes A, B, and C, respectively

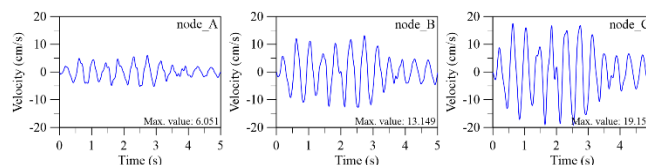


**Figure 16.** Time history velocities at nodes A, B, and C, respectively

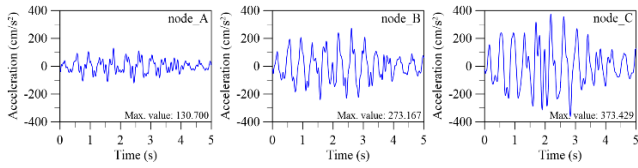


**Figure 17.** Time history acceleration at nodes A, B, and C, respectively

Figures 15-17 represent the displacement, velocity, and acceleration results at nodes A, B, and C, separately, for the uncontrolled situation of the building. Maximum displacement values were found as 0.357 cm, 0.861 cm and 1.221 cm while velocity values were calculated as 6.051 cm/s, 13.149 cm/s and 19.152 cm/s for node A, B and C, respectively. Also, maximum acceleration values of 130.700  $\text{cm/s}^2$ , 273.167  $\text{cm/s}^2$  and 373.429  $\text{cm/s}^2$  at node A, B and C were obtained. As can be seen from the figures, it is seen that the maximum vibration oscillation occurs at the top floor, and this oscillation is relatively lower on the first and second floors.

## 2.2 Dynamic earthquake analysis of seismic-isolated (passive earthquake controlled) RC building

In countries such as Turkey, where the majority of the population is at risk of earthquakes, the most critical natural event that should be considered in the design of almost all structures is the earthquake phenomenon. Depending on the gains obtained from years of experience, various studies have been carried out in earthquake engineering to protect structures against earthquake effects. One of the most important results of these studies, the concept of seismic isolation, also known as PEC, has emerged, and it has been widely preferred as a carrier system type, especially in the design of buildings. The seismic isolation system, based on the idea of separating the foundation and ground, is applied to the structure with different types of isolators, extending the period of the structure, reducing the incoming earthquake load, and reducing the relative story drift.

This study used HDRB to convert the existing building to a seismic isolation system. HDRB has been produced by the British institution "Malaysian Rubber Producer Research Association" against the disadvantages of low-damped and lead core isolators. The essential advantages of HDRB compared to other isolators can be listed as providing the necessary flexibility and damping without the need for another element, easy design, and easy production.

The effective behavior of the seismic isolation system in the event of an earthquake is highly dependent on the mechanical properties of the selected isolators. For this reason, it is essential to design a structure-specific isolator system instead of the existing isolators in the market. In this study, the design of building-specific HDRB was made by the Uniform Building Code (UBC-97) [53] and Turkey Earthquake Building Code (TEBC-2018) [54] criteria.

The steps followed in the design of high-damping rubber bearings are given below, step by step and in detail. Before starting the isolator design, it is necessary to collect some preliminary information required for the design. This information is used as input data in the isolator design. Data

are taken both from the structure and the relevant codes. The data taken for the design of HDRB are given in Table 4.

**Table 4.** Input data for HDRB design

First vibration period of the building ( $T_1$ )	0.412 s
Target (design) period ( $T_D$ )	1.236 s
Target maximum period ( $T_M$ )	1.5 s
Number of isolators	9 (total number of columns)
Total weight of the building ( $W$ )	1972.608 kN
Seismic zone factor ( $Z$ )	0.4 for 0.3-0.5g
Ground profile type	$S_D$ (Hard soil)
Seismic source type	A
Near-source factors	$N_v=1.6 / N_a=1.2$
Seismic coefficients	$C_{AM}=0.634 / C_{VM}=1.229$
Damping coefficient	$B_{D,M}=1.2$ ( $\beta_{D,M}=10\%$ )
Structural system behavior coefficient	$R=8.5 / R_1=2$

There are nine columns in total in the building. An isolator was placed under each column. The axial load on the columns is the primary data in the isolator design. Considering these data, it was seen that three different types of isolators were needed for the building; i) Type\_A for S01, S03, S05, and S07 columns, ii) Type\_B for S02, S04, S06, and S08 columns, iii) Type\_C for S05 column (Figure 18).

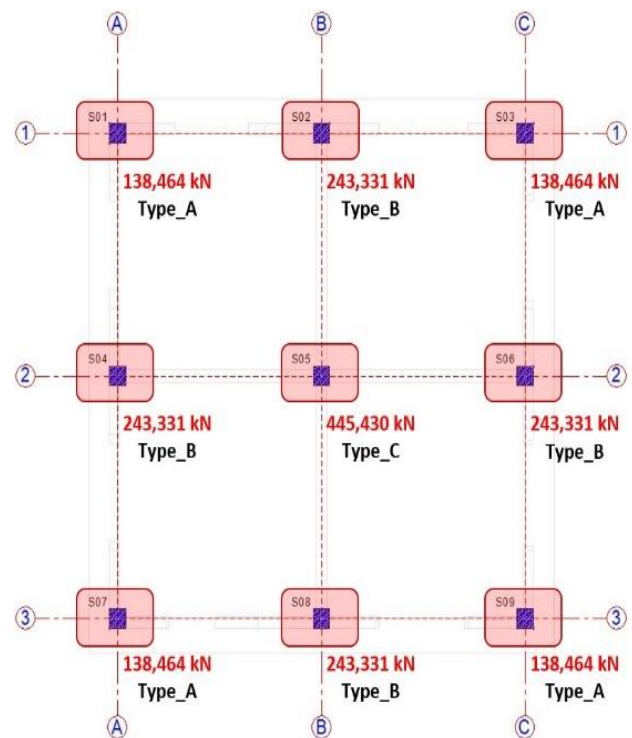


**Figure 18.** Axial loads on the columns and isolator types depending on this load

Considering the equations and criteria in the relevant codes, the mechanical properties defining the structural behavior of the HDRB in the event of an earthquake, in other words, the design outputs, were calculated and given in Table 5.

**Table 5.** Output data for HDRB design

Design displacement ( $D_D$ )	0.262 m
Maximum displacement ( $D_M$ )	0.382 m
Minimum horizontal stiffness ( $k_D$ )	364.746 kN/m for Type_A, 640.990 kN/m for Type_B 1173.365 kN/m for Type_C
Isolator height ( $t_r$ )	25 cm
Isolator diameter (R)	35 cm for Type_A 45 cm for Type_B 60 cm for Type_C
Horizontal stiffness ( $K_H$ )	384.845 kN/m for Type_A 636.173 kN/m for Type_B 1130.973 kN/m for Type_C
Effective vibration period ( $T_D$ )	1.231 s
Vertical stiffness ( $K_V$ )	105656.843 kN/m for Type_A 265409.582 kN/m for Type_B 722553.191 kN/m for Type_C
Vertical design displacement ( $\Delta t$ )	0.0009 m
Plastic stiffness ( $K_2$ )	384.845 kN/m for Type_A 636.173 kN/m for Type_B 1130.973 kN/m for Type_C
Elastic stiffness ( $K_1$ )	2309.070 kN/m for Type_A 3817.038 kN/m for Type_B 6785.838 kN/m for Type_C
Isolator shear force (Q)	48.462 kN for Type_A 85.166 kN for Type_B 155.901 kN for Type_C
Yield displacement ( $D_Y$ )	0.025 for Type_A 0.027 for Type_B 0.028 for Type_C
Equivalent stiffness ( $K_{eff}$ )	569.814 kN/m for Type_A 961.234 kN/m for Type_B 1726.015 kN/m for Type_C
Yield strength ( $F_Y$ )	57.727 kN for Type_A 103.060 kN for Type_B 190.003 kN for Type_C

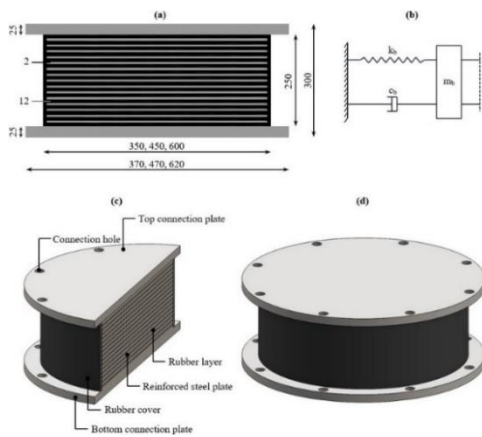


**Figure 19.** High damping rubber bearing (HDRB): (a) dimensional properties; (b) analytical model; (c) components; (d) three dimensional model

One of the crucial parameters describing the behavior of an isolator under the influence of earthquakes is the force-displacement curves. Force-displacement curves obtained for Type\_A, Type\_B, and Type\_C isolators are shown in Figure 20.

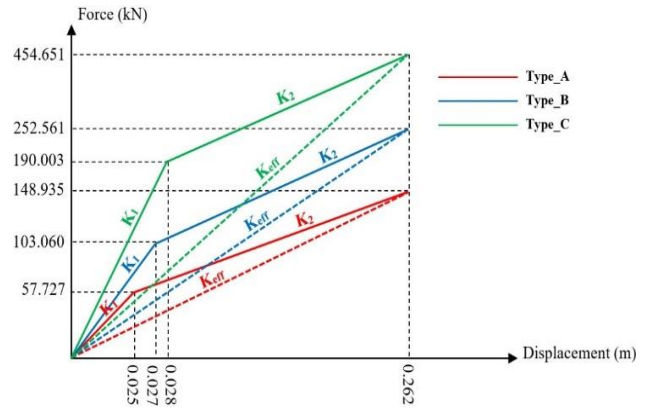


**Figure 20.** Force-displacement curves of isolators

The suitable element type for HDRB in ANSYS is COMBIN39. The non-linear behavior of the element operates only in static and non-linear transient dynamic analyses [58]. However, in this study, the linear dynamic analysis type was preferred for the reasons explained in the previous sections. The linear dynamic analysis for the whole structure in the SAP2000 program does not affect the non-linear behavior of the isolators. For this reason, the SAP2000 program was preferred in this section. According to the TEBC-2018, only the isolation units can be modeled for non-linear behavior in the building model, while the superstructure and substructure can be modeled as linear elastic [54].

Shell components represented slabs in the FEM, while frame elements represented beams and columns. The FEM had 381 connection points, 300 shell elements, and 153 frame elements. The model has dimensions of 10 m, 10 m, and 9 m in the X, Y, and Z axes, respectively (Figure 21).

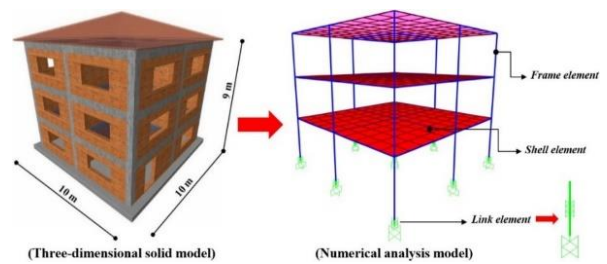


**Figure 21.** Three-dimensional solid and numerical models of the seismic-isolated RC building

For the frame, shell, and link elements on the numerical analysis model, FRAME, SHELL, and LINK objects from the SAP2000 library were preferred, respectively. The geometric properties of the elements are given in Figure 22.

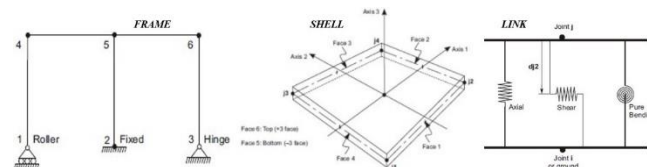


**Figure 22.** Geometric properties of FRAME, SHELL and LINK objects, respectively [57]

FRAME objects are straight lines connecting two nodes that model beams, columns, and truss elements in two- and three-dimensional systems. Torsion, axial deformation, biaxial bending, and biaxial shear are considered in the beam-column formulation characterizing the frame behavior [57].

SHELL objects with three or four nodes simulate the behavior of membranes and plates that bend. Shell objects help model components inside structural members of buildings, such as floors, walls, and 3D curved surfaces [57].

LINK objects connect two joints so that specialized structural behavior may be modeled. The SAP2000 program library has a special case of the LINK object defined for highly damped rubber bearings; High-Damping Rubber Isolator Link. This is a model for the high-damping rubber bearing in rubber isolators that undergo uniaxial or biaxial shear deformation. This model employs a time-independent deformation-history integral type model. The model's shear behavior is unaffected by axial deformation, while the axial behavior is linearly elastic [57].

Some mechanical properties of the isolator must be entered into the program to define HDRB in SAP2000. The considered mechanical properties for Type\_A, Type\_B, and Type\_C are given in Table 6.

Before making dynamic earthquake analyses in the time domain of the building, free vibration analysis of the structure was carried out to determine whether the effective vibration period (1.231 s) specified during the isolator's design phase could be reached. As a result of the analysis showed that the vibration period of the seismic-isolated RC concrete building was 1.205 seconds, with an error rate of approximately 2% (Figure 23). This indicates that the isolator has been modeled correctly and exhibits the targeted structural behavior.

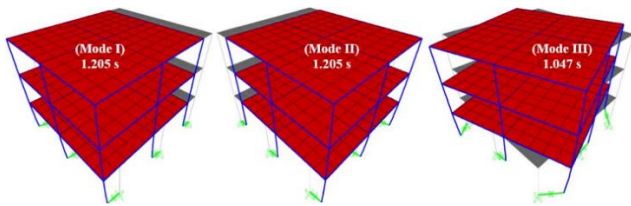


Figure 23. The first three mod shapes of the seismic-isolated RC building

Linear dynamic earthquake analyses in the time history of the building were performed using the Acc\_E record of the Seferihisar (İzmir) earthquake with the help of the SAP2000 program. The earthquake effect was applied in the X-direction, which is the dominant vibration mode direction of the structure. As a result of the analysis, the maximum displacement, velocity, and acceleration values along the height of the structure were obtained as the earthquake

behavior parameters of the building. Besides, displacement, velocity, and acceleration values read in time history from A, B, and C nodes were taken. These results are shown in Figures 24-27.

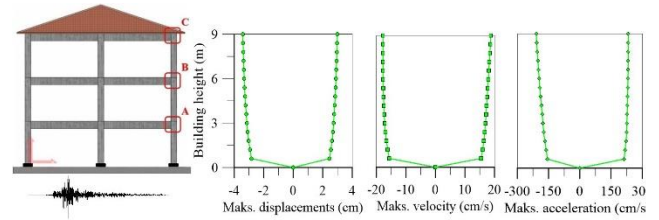


Figure 24. Distribution of maximum displacement, velocity and acceleration values along the height of the building

Figure 24 indicates the maximum amplitudes of displacement, velocity, and acceleration responses at each node along the stories in the building. For PEC, maximum displacement, velocity, and acceleration values are approximately  $\pm 4$  cm,  $\pm 20$  cm/s, and  $\pm 300$  cm/s<sup>2</sup>, respectively. As seen in Figure 24, the vibration amplitudes are distributed almost as a constant value along the height of the building. Thus, the relative structural behavior remains at low levels, and accordingly, there are significant decreases in the values of the internal structural forces. This is expected behavior from a seismically isolated system.

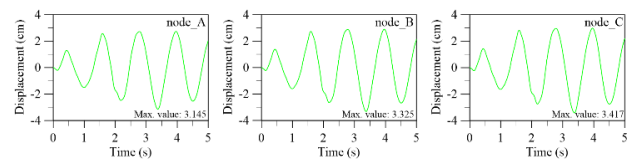


Figure 25. Time history displacements at nodes A, B, and C, respectively

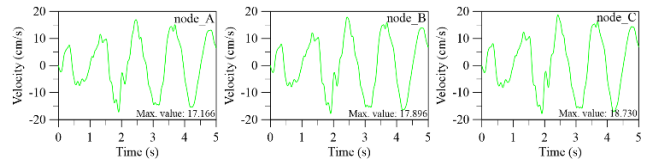


Figure 26. Time history velocities at nodes A, B, and C, respectively

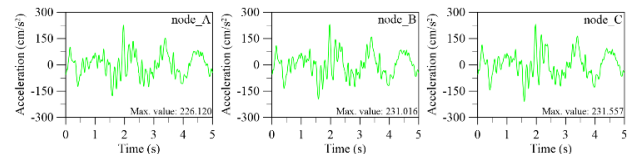


Figure 27. Time history acceleration at nodes A, B, and C, respectively

Table 6. Mechanical properties of isolators.

Isolator Type	Vertical Stiffness [kN/m]		Horizontal Stiffness [kN/m]		Yield Strength [kN]		K <sub>2</sub> /K <sub>1</sub>	
	Linear	Nonlinear	Linear	Nonlinear	Linear	Nonlinear	Linear	Nonlinear
Type_A	105656.843	-	569.814	2309.07	-	57.727	-	0.167
Type_B	265409.582	-	961.234	3817.038	-	103.060	-	0.167
Type_C	722553.191	-	1726.015	6785.838	-	190.003	-	0.167

Figures 25-27 represent the displacement, velocity, and acceleration results at nodes A, B, and C, separately, for the PEC situation of the building. Maximum displacement values were found as 3.145 cm, 3.325 cm and 3.417 cm while velocity values were calculated as 17.166 cm/s, 17.896 cm/s and 18.730 cm/s for node A, B and C, respectively. Also, maximum acceleration values of 226.120 cm/s<sup>2</sup>, 231.016 cm/s<sup>2</sup> and 231.557 cm/s<sup>2</sup> at node A, B and C were obtained. As can be seen from the figures, it is seen that the maximum vibration oscillation occurs on the top floor, but there is no significant difference between floors in terms of these values.

### 2.3 Analysis of active earthquake control

In this section, the active force-based and displacement-based control designs were proposed with acceleration and displacement feedback. The control design was adopted for the proportional-integral-derivative (PID) control system used for a three-story building excited to the earthquake.

The active control block diagram is shown in Figure 28.

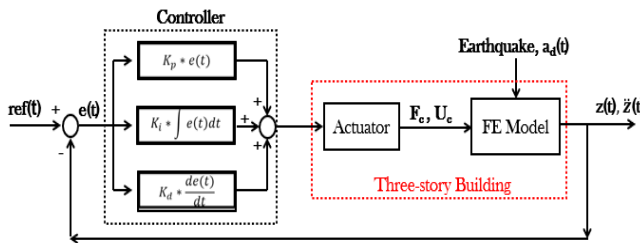


Figure 28. Active control block diagram

In the block diagram,  $ref(t)$  is defined as the reference signal, which is equal to zero to eliminate the vibrations from earthquake excitation.  $e(t)$  is the error signal, while the displacement and acceleration signals are denoted by  $z(t)$  and  $\ddot{z}(t)$ , respectively. The force-based  $F_c$  and displacement-based  $U_c$  actuators were chosen for AEC, while the earthquake excitation  $a_d(t)$  was the disturbance input. Closed-loop control was realized in the FE solution in ANSYS. Nodes of inputs and outputs in the FE model are defined as shown in Figure 29.

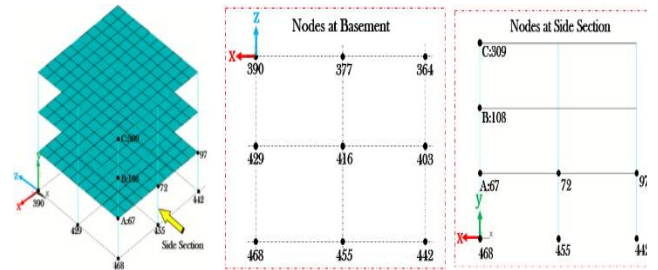


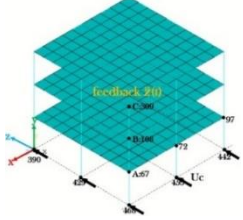
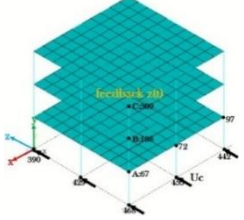
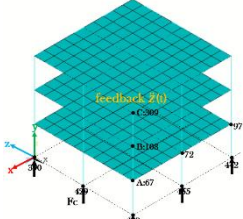
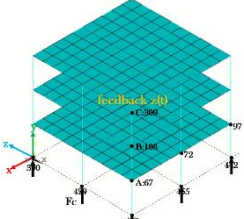
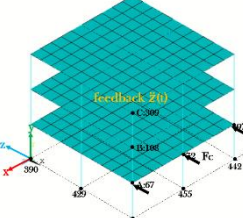
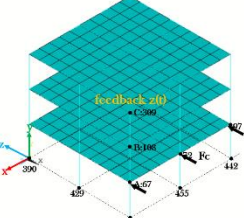
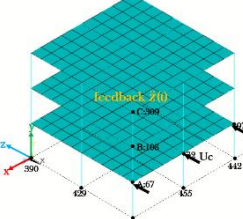
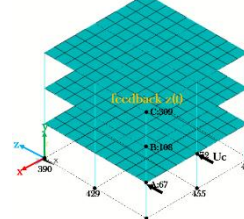
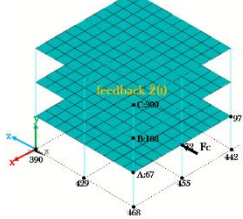
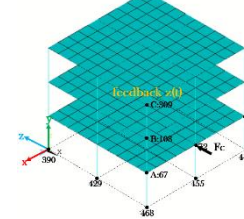
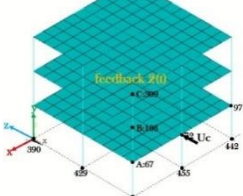
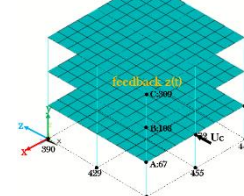
Figure 29. Defining nodes for AEC

Figure 29 indicates the determined nodes for the AEC. Nodes A, B, and C numbers 67, 108, and 309 are the displacement, acceleration, and velocity response nodes of the first, second, and third floors, separately. Also, node C was selected as the feedback node to reduce the vibrations on the high floor of a three-story building. Earthquake excitation was applied to the nodes (390, 377, 364, 429, 416, 403, 468, 455, and 442) at the basement of the building to define the ground motion. The force-based and displacement-based actuators were utilized with acceleration and displacement feedback signals. The configuration of the actuators and feedback signals shown in Table 7 is specified to determine the best control performance for the optimum actuator location and feedback types.

All fourteen configurations were determined according to the actuator type and location using displacement and acceleration feedback. For example, for Configuration-1 (C1), the actuator type was selected as the forced-based  $F_c$  actuator in the z-direction, while all nodes in the basement were used for the actuator location. The acceleration signal at node C was used for feedback in AEC. Similarly, the actuator type and location for C14 were defined as the displacement-based  $U_c$  actuator in node 72. At the same time, the feedback signal was the displacement signal at node C. Generally, the acceleration or displacement vibration responses in the z-direction at node C were denoted as feedback for all configurations. To evaluate the effectiveness of AEC for all configurations, the displacement, velocity, and acceleration responses of nodes A, B, and C were selected as response nodes.

Table 7. Configuration of the actuator type with the applied location and the selected feedback

Configuration-1 (C1)		Configuration-2 (C2)	
	Actuator type: <b>F<sub>c</sub> (z-direction)</b> All nodes at Basement		Actuator type: <b>F<sub>c</sub> (z-direction)</b> All nodes at Basement
	Feedback: <b><math>\ddot{z}(t)</math> at node C</b>		Feedback: <b><math>z(t)</math> at node C</b>
Configuration-3 (C3)		Configuration-4 (C4)	
	Actuator type: <b>U<sub>c</sub> (z-direction)</b> All nodes at Basement		Actuator type: <b>U<sub>c</sub> (z-direction)</b> All nodes at Basement

	Feedback: $\ddot{z}(t)$ at node C		Feedback: $z(t)$ at node C
<b>Configuration-5 (C5)</b>		<b>Configuration-6 (C6)</b>	
	Actuator type: <b>Fc (y-direction)</b> All nodes at Basement		Actuator type: <b>Fc (y-direction)</b> All nodes at Basement
Feedback: $\ddot{z}(t)$ at node C		Feedback: $z(t)$ at node C	
<b>Configuration-7 (C7)</b>		<b>Configuration-8 (C8)</b>	
	Actuator type: <b>Fc (z-direction)</b> Nodes 67, 72, 97		Actuator type: <b>Fc (z-direction)</b> Nodes 67, 72, 97
Feedback: $\ddot{z}(t)$ at node C		Feedback: $z(t)$ at node C	
<b>Configuration-9 (C9)</b>		<b>Configuration-10 (C10)</b>	
	Actuator type: <b>Uc (z-direction)</b> Nodes 67, 72, 97		Actuator type: <b>Uc (z-direction)</b> Nodes 67, 72, 97
Feedback: $\ddot{z}(t)$ at node C		Feedback: $z(t)$ at node C	
<b>Configuration-11 (C11)</b>		<b>Configuration-12 (C12)</b>	
	Actuator type: <b>Fc (z-direction)</b> Node 72		Actuator type: <b>Fc (z-direction)</b> Node 72
Feedback: $\ddot{z}(t)$ at node C		Feedback: $z(t)$ at node C	
<b>Configuration-13 (C13)</b>		<b>Configuration-14 (C14)</b>	
	Actuator type: <b>Uc (z-direction)</b> Node 72		Actuator type: <b>Uc (z-direction)</b> Node 72
Feedback: $\ddot{z}(t)$ at node C		Feedback: $z(t)$ at node C	

A macro code in the transient analysis was integrated into the FE analysis in ANSYS for the AEC action. The earthquake excitation was applied to the basement nodes at each time step. Then, the active control loop began at time  $t=dt$  in transient analysis after the feedback signal  $yf(t)$  is read from the feedback node with the following macro code: “\*get,dz,node,309,u,z” for displacement feedback, and

“\*get,az,node,309,a,z” for acceleration feedback.  $dt$  is the time step.  $e(t)$  is calculated as  $e(t)=ref(t)-yf(t)$ . In order to obtain the actuator signal  $u(t)$ ,  $e(t)$  is multiplied by proportional gain  $K_p$ , its integral is multiplied by integral gain  $K_i$ , its derivative is multiplied by derivative gain  $K_d$ . Then,  $u(t)$  is calculated by summing these signals.  $K_p$ ,  $K_i$ , and  $K_d$  are defined as the controller gains. For  $F_c$  and  $U_c$ ,

the actuator signal is found. According to the forced-based and displacement-based actuators,  $F_c$  or  $U_c$  are applied to the three-story buildings. Then, the closed-loop with “\*do\*  
\*enddo” command proceeds until the steady-state value of the system is attained the number of samples through the defined analysis time. The macro program for the active control was developed with ANSYS Parametric Design Language.

The AEC control with the acceleration and displacement feedback was performed for the selected actuator locations in different configurations using FE analysis. Closed-loop control implementation was carried out with two different actuator types force-based and displacement-based. Firstly, controller gains were found by using the trial-and-error method. Then, according to the feedback signal and vibration responses at response nodes, controller gains were optimized with minimum displacement and acceleration vibration responses. When the active analysis results were compared according to the actuator locations and the feedback signals, the best vibration suppression results were found for C13, obtained in the vibration results of the displacement-based actuator used at node 72. With the AEC for C13, the maximum displacement, velocity, and acceleration values along the height of the structure with controller gains of  $K_p=0.000015$ ,  $K_i=0$ , and  $K_d=0.0000002$  were obtained as shown in Fig. 30. Also, the displacement, velocity, and acceleration responses obtained from nodes A, B, and C for the first, second, and third floors of the building are shown in Figures 30-33.

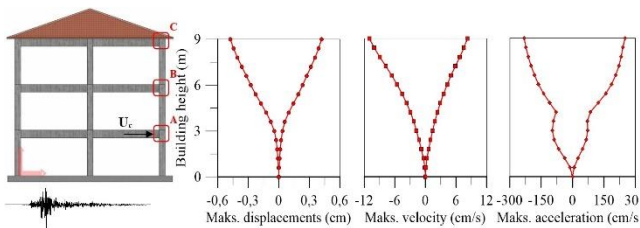


**Figure 30.** Distribution of maximum displacement, velocity and acceleration values along the height of the building

Figure 30 indicates the maximum amplitudes of displacement, velocity, and acceleration responses at each node along the stories in the building. For the AEC, maximum displacement, velocity, and acceleration values were approximately  $\pm 5$  cm,  $\pm 12$  cm/s, and  $\pm 225$  cm/s<sup>2</sup>, respectively. As seen in Figure 30, the amplitudes of vibrations are the highest for the top floor in the building, while those are relatively lower for the first and second floors according to the top point of the building.

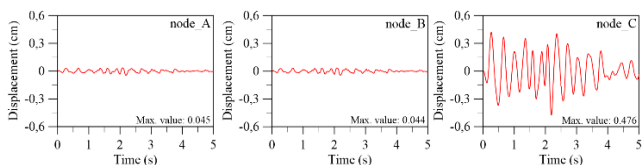


**Figure 31.** Time history displacements at nodes A, B, and C, respectively

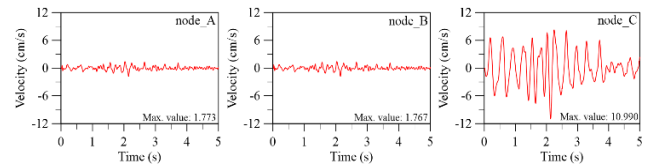


**Figure 32.** Time history velocities at nodes A, B, and C, respectively

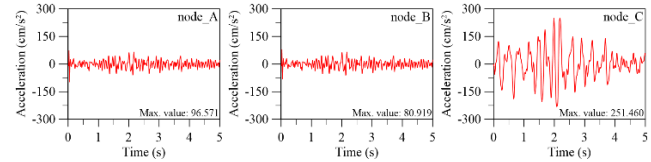


**Figure 33.** Time history acceleration at nodes A, B, and C, respectively

Figures 31-33 separately represent the displacement, velocity, and acceleration results at nodes A, B, and C for the actuator location, and acceleration feedback obtained better control performance. For the AEC of the building, maximum displacement values were found as 0.045 cm, 0.044 cm, and 0.476 cm, while velocity values of 1.773 cm/s, 1.767 cm/s, and 10.990 cm/s for nodes A, B, and C, respectively. Also, maximum acceleration values 96.571 cm/s<sup>2</sup>, 80.919 cm/s<sup>2</sup>, and 251.460 cm/s<sup>2</sup> at nodes A, B, and C were obtained. As seen from the figures, it is clear that the maximum vibration oscillation occurs at the top floor, and this oscillation on the first and second floors is relatively weak.

To comparatively evaluate the performance of PEC and AEC, the distribution of the maximum displacement, velocity, and acceleration values that occurred at all nodes along the height of the building is given in Figure 34.

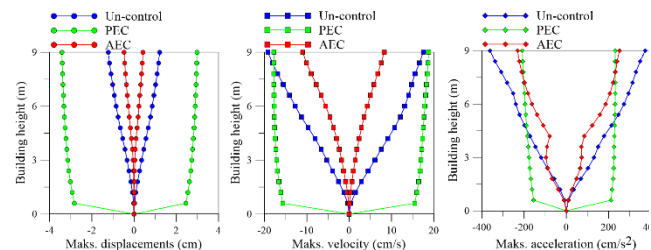


**Figure 34.** Comparative distribution of maximum displacement, velocity and acceleration values along the height of the building

Figure 34 shows the comparative distribution of the maximum displacement, velocity, and acceleration response values for all three cases along the building height.

When the displacement behavior of the building is examined, AEC reduces the displacement value at every point along the height of the building. The displacement distribution is approximately linearly parallel to the uncontrolled state. In the case of PEC, on the contrary, the displacement value increases at every point, and displacement distribution proceeds at an approximately constant value along the height of the building. This distribution is expected behavior from seismic isolated buildings. The critical issue here is that these displacements are between the limit values determined by the regulations.

In addition, the relative story drifts remain at minimal values in both control conditions. This situation ensures that the internal forces formed in the carrier system elements take small values. Regarding displacement behavior, it can be said that AEC provides better earthquake behavior than PEC.

When the velocity responses of the building are examined, a similar situation is observed with the displacement behavior. AEC significantly reduces the velocity value at every point along the height of the building. In the case of PEC, there is an increase in the speed value on the first two floors of the building and a slight decrease in this value on the top floor. As the height of the building increases, there is a noticeable increase in the effectiveness of the PEC. Regarding velocity behavior, it can be said that AEC provides better earthquake behavior on lower floors than PEC, which can be an essential alternative to PEC on upper floors.

When the acceleration responses of the building are examined, the AEC decreases the acceleration value at every point along the height of the building. The same is true for PEC on other floors except for the first floor. The maximum acceleration values obtained for both AEC and PEC on the top floor of the building are almost the same. As the height of the building increases, there is a noticeable increase in the effectiveness of the PEC. In the AEC, the same is true for all floors. Regarding acceleration behavior, it can be said that AEC provides better earthquake behavior on lower floors than PEC, which can be an essential alternative to PEC on upper floors. A vital issue to note here is that there is a critical region slightly above the point where AEC is applied. From this region, the rate of decrease in the acceleration value decreases. The place where AEC is used significantly affects the behavior of the building at the time of the earthquake. For this reason, in this study, a parametric study was carried out to determine the appropriate location for AEC, and the results are given in full detail in the following sections.

When all three graphs are evaluated together, it can be said that AEC is a very effective method for improving the seismic behavior of an RC building.

For the comparative evaluation of PEC and AEC performance, the displacement, velocity, and acceleration values in the time history were read from the nodes A, B, and C located on the first, second, and third floors of the building, respectively, are given in Figures 35-37.

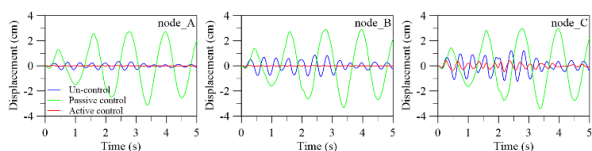


**Figure 35.** Comparative time history displacements at nodes A, B, and C, respectively

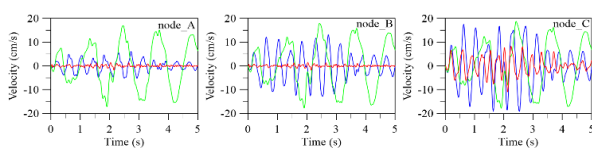


**Figure 36.** Comparative time history velocities at nodes A, B, and C, respectively

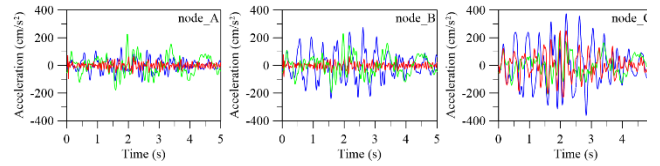


**Figure 37.** Comparative time history acceleration at nodes A, B, and C, respectively

Figures 35-37 present the time-dependent displacement, velocity, and acceleration changes at nodes A, B, and C, respectively. It is seen that AEC causes a significant decrease in the structural response values occurring on all floors of the building at each step within the considered time interval. This situation reveals that AEC is a very effective method to improve the structural behavior of an RC building during an earthquake.

### 2.3.1 Results of case studies for AEC

Case studies for configurations given in Table 7 were realized to determine the best vibration minimization performance of the AEC. Vibration responses for different actuator types and locations were obtained for different feedback signals. The displacement, velocity, and acceleration responses of the top floor of the building were evaluated as performance criteria of the designed controller. Controller gains were optimized until the best performance was achieved for vibration responses. Case results for all configurations were obtained. Firstly, for C1 with controller gains of  $K_p=1.25 \times 10^3$ ,  $K_i=80$ , and  $K_d=10$ , displacement, velocity, and acceleration results are shown in Figure 38.

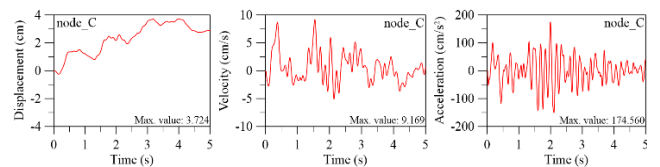


**Figure 38.** Time history displacement, velocity and acceleration responses for C1 at nodes A, B, and C, respectively

Figure 38 shows the displacement, velocity, and acceleration responses of the top floor in the building for C1. From Fig. 38, maximum velocity and acceleration values are reduced from 19.152 cm/s and 373.42 cm/s<sup>2</sup> to 9.169 cm/s and 174.560 cm/s<sup>2</sup>, respectively, while this value of displacement is increased from 1.221 cm to 3.724 cm. Even though the maximum velocity and acceleration values are reduced with AEC, the C1 configuration is unsuitable because the maximum displacement values are increased, and the vibration behavior of displacement responses is unacceptable for earthquake vibration damping.

The vibration responses for another configuration, C3 are shown in Figure 39 for the controller gains of  $K_p=2 \times 10^{-3}$ ,  $K_i=1 \times 10^{-3}$  and  $K_d=1 \times 10^{-5}$ .

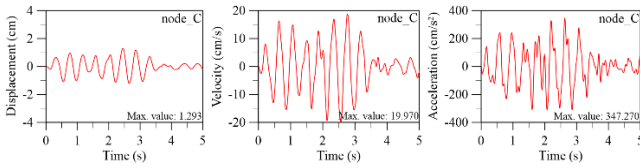


**Figure 39.** Time history displacement, velocity and acceleration responses for C3 at nodes A, B, and C, respectively

For the C3 configuration, it is observed from Figure 39 that all maximum values are increased according to reference values. Therefore, it can be seen that the C3 configuration is not a suitable method for active earthquake control depending on the actuator location and type and also the feedback selected.

For C2, C4, C5-8, C10, C14, the vibration responses of top floor are obtained and shown in Figures. 40-46.

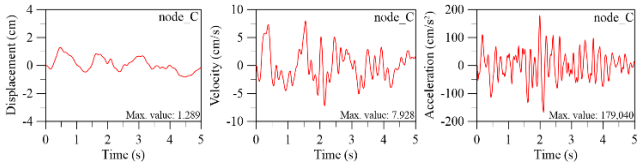


**Figure 40.** Time history displacement, velocity and acceleration responses for C2 at nodes A, B, and C, respectively, the controller gains of  $K_p=8 \times 10^4$ ,  $K_i=5 \times 10^3$  and  $K_d=3 \times 10^4$

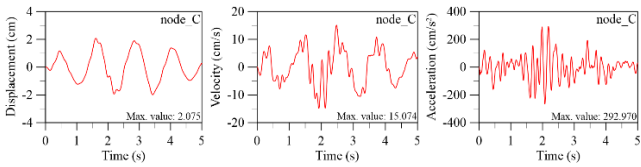


**Figure 41.** Time history displacement, velocity and acceleration responses for C5 at nodes A, B, and C, respectively, the controller gains of  $K_p=1 \times 10^5$ ,  $K_i=0$  and  $K_d=0$

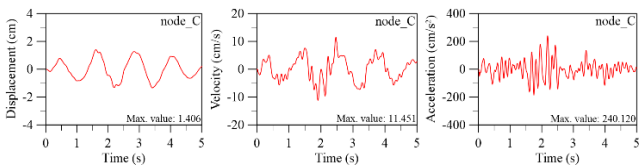


**Figure 42.** Time history displacement, velocity and acceleration responses for C6 at nodes A, B, and C, respectively, the controller gains of  $K_p=1 \times 10^{10}$ ,  $K_i=0$  and  $K_d=0$

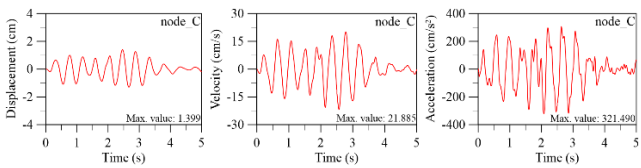


**Figure 43.** Time history displacement, velocity and acceleration responses for C7 at nodes A, B, and C, respectively, the controller gains of  $K_p=1 \times 10^4$ ,  $K_i=1 \times 10^3$  and  $K_d=2 \times 10^2$

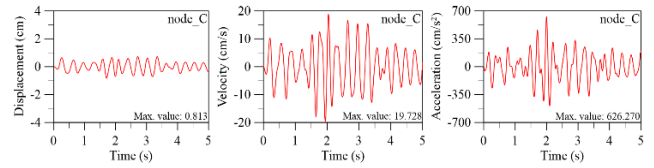


**Figure 44.** Time history displacement, velocity and acceleration responses for C8 at nodes A, B, and C, respectively, the controller gains of  $K_p=2 \times 10^7$ ,  $K_i=5 \times 10^6$  and  $K_d=1 \times 10^5$

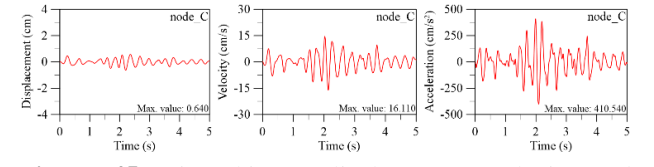


**Figure 45.** Time history displacement, velocity and acceleration responses for C10 at nodes A, B, and C, respectively, the controller gains of  $K_p=2 \times 10^{-2}$ ,  $K_i=0$  and  $K_d=1 \times 10^{-3}$

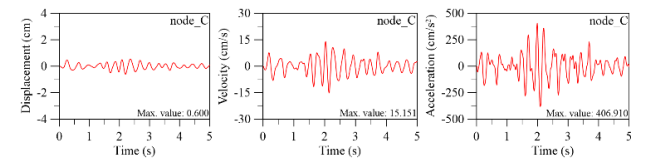


**Figure 46.** Time history displacement, velocity and acceleration responses for C14 at nodes A, B, and C, respectively, the controller gains of  $K_p=2 \times 10^{-2}$ ,  $K_i=1 \times 10^2$  and  $K_d=1 \times 10^{-3}$

As seen from Figures 40-46, the controller gains are different for all configurations. For example, for C2 with the controller gains of  $K_p=8 \times 10^4$ ,  $K_i=5 \times 10^3$  and  $K_d=3 \times 10^4$ , maximum values are changed from 1.221 cm, 19.152 cm/s, 373.42 cm/s<sup>2</sup> to 1.289 cm, 7.928 cm/s, 179.040 cm/s<sup>2</sup> for displacement, velocity and acceleration responses, separately. For C2, C5, and C6 configurations, despite the decrease in acceleration and velocity values, it is clear that the displacement values according to controlled reference values of C13 are still not at the desired values. Also, for C10 and C14, maximum displacement and velocity values are reduced depending on reference values while maximum acceleration value is increased. For C7 and C8, maximum velocity values are increased; however, the maximum displacement value for C7 is increased according to reference values while this value for C8 is decreased.

For C4, C9, C11-12, the displacement, velocity and acceleration vibration responses of top floor are obtained with different controller gains and shown in Figures 47-50.

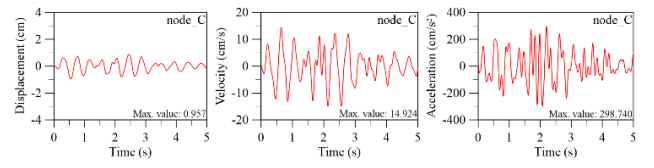


**Figure 47.** Time history displacement, velocity and acceleration responses for C4 at nodes A, B, and C, respectively, the controller gains of  $K_p=5 \times 10^{-2}$ ,  $K_i=5 \times 10^3$  and  $K_d=5 \times 10^{-3}$

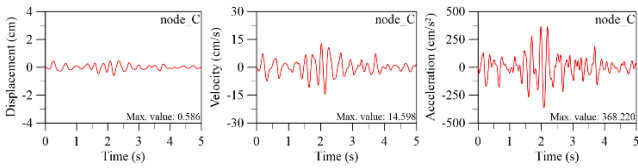


**Figure 48.** Time history displacement, velocity and acceleration responses for C9 at nodes A, B, and C, respectively, the controller gains of  $K_p=1 \times 10^{-6}$ ,  $K_i=0$  and  $K_d=1 \times 10^{-8}$

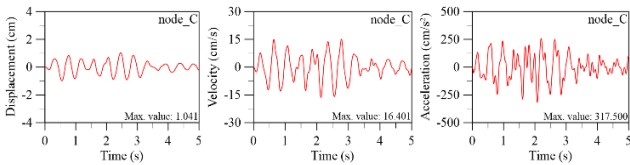


**Figure 49.** Time history displacement, velocity and acceleration responses for C11 at nodes A, B, and C, respectively, the controller gains of  $K_p=3 \times 10^4$ ,  $K_i=2 \times 10^5$  and  $K_d=1 \times 10^2$

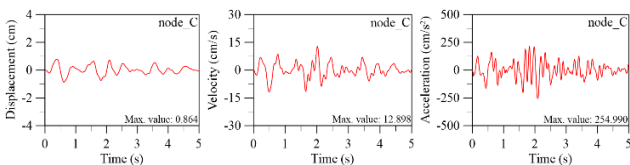


**Figure 50.** Time history displacement, velocity and acceleration responses for C12 at nodes A, B, and C, respectively, the controller gains of  $K_p=5 \times 10^7$ ,  $K_i=1 \times 10^7$  and  $K_d=6 \times 10^5$

As seen from Figures 47-50, it can be seen that maximum values of displacements, velocities, and accelerations for all configurations are reduced with respect to the maximum values of uncontrolled vibration responses in the building. For example, for C12 configuration, maximum displacement, velocity and acceleration values are reduced from 1.221 cm, 19.152 cm/s, 373.42 cm/s<sup>2</sup> to 0.864 cm, 12.898 cm/s, 254.990 cm/s<sup>2</sup> for responses, respectively. Although maximum values for C4, C9, C11-12 are shown in Figures 47-50 are reduced for displacement, velocity, and acceleration responses, the effectiveness of control performance is not sufficient when comparing maximum values of C4, C9, C11-12 with C13.

### 3 Conclusions

In this paper, a numerical study was carried out on the effectiveness of the active earthquake control method (AEC), which is thought to be an alternative to the seismic isolation (passive earthquake control) method (PEC), in improving the earthquake response of RC buildings.

When the graphs that present the results comparatively are examined, the following basic conclusions are reached;

- Maximum displacement values at node A on the first floor of the building are read as 0.357 cm, 3.145 cm, and 0.045 cm for uncontrolled, passive earthquake-controlled, and active earthquake-controlled

situations, respectively. PEC increased this value approximately 8.81 times, while AEC decreased this value by about 7.93 times.

- Maximum displacement values at node B on the second floor of the building are read as 0.861 cm, 3.325 cm, and 0.044 cm for uncontrolled, passive earthquake-controlled, and active earthquake-controlled situations, respectively. PEC increased this value approximately 3.86 times, while AEC decreased this value by about 19.57 times.
- Maximum displacement values at node C on the top floor of the building are read as 1.221 cm, 3.417 cm, and 0.476 cm for uncontrolled, passive earthquake-controlled, and active earthquake-controlled situations, respectively. PEC increased this value approximately 2.80 times, while AEC decreased this value by about 2.57 times.

When the displacement behavior of the building is examined, active control significantly reduces the displacement value on each floor. In the case of PEC, on the contrary, the displacement value increases. Also, the relative story drifts remain at minimum values in both control conditions. This situation ensures that the internal forces formed in the carrier system elements take small values. Regarding displacement behavior, it can be said that AEC provides better earthquake behavior than PEC

- Maximum velocity values at node A on the first floor of the building are read as 6.051 cm/s, 17.166 cm/s, and 1.773 cm/s for uncontrolled, passive earthquake-controlled, and active earthquake-controlled situations, respectively. PEC increased this value approximately 2.84 times, while AEC decreased this value by about 3.41 times.
- Maximum velocity values at node B on the second floor of the building are read as 13.149 cm/s, 17.896 cm/s, and 1.767 cm/s for uncontrolled, passive earthquake-controlled, and active earthquake-controlled situations, respectively. PEC increased this value approximately 1.36 times, while AEC decreased this value by about 7.44 times.
- Maximum velocity values at node C on the top floor of the building are read as 19.152 cm/s, 18.730 cm/s, and 10.990 cm/s for uncontrolled, passive earthquake-controlled, and active earthquake-controlled situations, respectively. PEC decreased this value approximately 1.02 times, while AEC decreased this value by about 1.74 times.

When the velocity responses of the building are examined, AEC significantly reduces the velocity value on each floor. In the case of PEC, there is an increase in the speed value on the first two floors of the building and a slight decrease in this value on the top floor. As the height of the building increases, there is a noticeable increase in the effectiveness of the PEC. Regarding velocity behavior, it can be said that AEC provides better earthquake behavior on lower floors than PEC, which can be an essential alternative to PEC on upper floors.

- Maximum acceleration values at node A on the first floor of the building are read as 130.700 cm/s<sup>2</sup>,

226.120 cm/s<sup>2</sup>, and 96.571 cm/s<sup>2</sup> for uncontrolled, passive earthquake-controlled, and active earthquake-controlled situations, respectively. PEC increased this value approximately 1.73 times, while AEC decreased this value by about 1.35 times.

- Maximum acceleration values at node B on the second floor of the building are read as 273.167 cm/s<sup>2</sup>, 231.016 cm/s<sup>2</sup>, and 80.919 cm/s<sup>2</sup> for uncontrolled, passive earthquake-controlled, and active earthquake-controlled situations, respectively. PEC decreased this value approximately 1.18 times, while AEC decreased this value by about 3.38 times.
- Maximum acceleration values at node C on the top floor of the building are read as 373.429 cm/s<sup>2</sup>, 231.557 cm/s<sup>2</sup>, and 251.460 cm/s<sup>2</sup> for uncontrolled, passive earthquake-controlled, and active earthquake-controlled situations, respectively. PEC decreased this value approximately 1.61 times, while AEC decreased this value by about 1.49 times.

When the acceleration responses of the building are examined, the AEC decreases the acceleration value on each floor. The same is true for PEC on other floors except for the first floor. The maximum acceleration values obtained for both AEC and PEC on the top floor of the building are almost the same. As the height of the building increases, there is a noticeable increase in the effectiveness of the PEC. In AEC, the same is true for all floors. Regarding acceleration behavior, it can be said that AEC provides better earthquake behavior on lower floors than PEC, which can be an essential alternative to PEC on upper floors.

The AEC method provides almost all the positive behaviors expected from the PEC method. In addition, it eliminates some disadvantages of the PEC method. E.g., a PEC system causes large displacements in the building. If the displacement values exceed the limit values the regulations allow, risky situations may arise for the building. The AEC method significantly limits the displacements along the height of the building. In this way, this dangerous situation is wholly eliminated. Besides, isolators cannot be partially applied to a building. It is applied to the building as an isolation system, that is, as an isolator group. Therefore, efficient implementation is complex and requires highly skilled workers and engineers. In addition, this situation and the costs of the insulators increase the total construction cost. AEC with an actuator from a single point provides ease of application and cost reduction.

#### Conflict of interest

The authors affirm that none of their known financial conflicts of interest or personal connections could have appeared to impact the research presented in this study.

**Similarity rate (iThenticate):** 18%

#### References

- [1] Geology.com. <https://geology.com/plate-tectonics.shtml>, Accessed 1 October 2022.
- [2] Global Earthquake Hazard Map. <https://www.globalquakemodel.org/gem-maps/global-earthquake-hazard-map>, Accessed 1 October 2022.
- [3] A. Ellero, G. Ottria, M. Marroni, L. Pandolfi and M. C. Göncüoğlu, Analysis of the North Anatolian Shear Zone in Central Pontides (northern Turkey): Insight for geometries and kinematics of deformation structures in a transpressional zone. *Journal of Structural Geology*, 72, 124–41, 2015. <https://doi.org/10.1016/j.jsg.2014.12.003>.
- [4] V. A. Zayas, S. S. Low and S. A. Mahin, A simple pendulum technique for achieving seismic isolation. *Earthquake Spectra*, 6, 317–33, 1990. <https://doi.org/10.1193/1.15855>.
- [5] M. Constantinou, A. Mokha and A. Reinhorn, Teflon bearings in base isolation II: Modeling. *Journal of Structural Engineering*, 116 (2), 455–74, 1990. [https://doi.org/10.1061/\(ASCE\)07339445\(1990\)116:2\(455\)](https://doi.org/10.1061/(ASCE)07339445(1990)116:2(455)).
- [6] D. V. Achillopoulou and N. K. Stamataki, Seismic design and assessment of the response of a glass pavilion. *Journal of Building Engineering*, 47, 103825, 2022. <https://doi.org/10.1016/j.job.2021.103825>.
- [7] N. Güneş, Risk-targeted design of seismically isolated buildings. *Journal of Building Engineering*, 46, 103665, 2022. <https://doi.org/10.1016/j.job.2021.103665>.
- [8] J. Shang, P. Tan, J. Han, Y. Zhang and Y. Li, Performance of seismically isolated buildings with variable friction pendulum bearings under near-fault ground motions. *Journal of Building Engineering*, 45, 103584, 2022. <https://doi.org/10.1016/j.job.2021.103584>.
- [9] E. Ozer, M. Inel and B. T. Cayci, Seismic behavior of LRB and FPS type isolators considering torsional effects. *Structures*, 37, 267–83, 2022. <https://doi.org/10.1016/j.istruc.2022.01.011>.
- [10] T. Sheng, G. bin Liu, X. cheng Bian, W. xing Shi and Y. Chen, Development of a three-directional vibration isolator for buildings subject to metro and earthquake-induced vibrations. *Engineering Structures*, 252, 1–31, 2022. <https://doi.org/10.1016/j.engstruct.2021.113576>.
- [11] S. Kitayama and M. C. Constantinou, Performance evaluation of seismically isolated buildings near active faults. *Earthquake Engineering & Structural Dynamics*, 51 (5), 1017–37, 2022. <https://doi.org/10.1002/eqe.3602>.
- [12] J. C. Reyes, Seismic behaviour of torsionally-weak buildings with and without base isolators. *Seismic Behaviour and Design of Irregular and Complex Civil Structures IV, Part of the Geotechnical, Geological and Earthquake Engineering book series (GGEE)*, 50, 177–88, 2022.
- [13] T. M. Al-Hussaini, M. M. Hoque and A. S. Moghadam, Seismic strengthening solutions for existing buildings. *Civil Engineering for Disaster Risk Reduction, Part of the Springer Tracts in Civil Engineering Book Series (SPRTRCIENG)*, 359–72, 2022.
- [14] S. Kitayama and H. Cilsalar, Seismic loss assessment of seismically isolated buildings designed by the procedures of ASCE/SEI 7-16. *Bulletin of Earthquake*

- Engineering, 20, 1143–68, 2022. <https://doi.org/10.1007/s10518-021-01274-y>.
- [15] H. Du, Y. Wang, M. Han and L. F. Ibarra, Experimental seismic performance of a base-isolated building with displacement limiters. *Engineering Structures*, 244, 112811, 2021. <https://doi.org/10.1016/j.engstruct.2021.112811>.
- [16] R. Astroza, J. P. Conte, J. I. Restrepo, H. Ebrahimi and T. Hutchinson, Seismic response analysis and modal identification of a full-scale five-story base-isolated building tested on the NEES@UCSD shake table. *Engineering Structures*, 238, 112087, 2021. <https://doi.org/10.1016/j.engstruct.2021.112087>.
- [17] A. Di Cesare, F. C. Ponzo and A. Telesca, Improving the earthquake resilience of isolated buildings with double concave curved surface sliders. *Engineering Structures*, 228, 111498, 2021. <https://doi.org/10.1016/j.engstruct.2020.111498>.
- [18] E. Meral, Determination of seismic isolation effects on irregular RC buildings using friction pendulums. *Structures*, 34, 3436–52, 2021. <https://doi.org/10.1016/j.istruc.2021.09.062>.
- [19] F. Mazza and M. Mazza, Nonlinear modelling of HDRBs in the seismic analysis of retrofitted and new base-isolated r.c. buildings. *Structures*, 33, 4148–61, 2021. <https://doi.org/10.1016/j.istruc.2021.07.010>.
- [20] N. Güneş and Z. Ç. Ulucan, Collapse probability of code-based design of a seismically isolated reinforced concrete building. *Structures*, 33, 2402–12, 2021. <https://doi.org/10.1016/j.istruc.2021.06.010>.
- [21] X. Wang, L. Xie, D. Zeng, C. Yang and Q. Liu, Seismic retrofitting of reinforced concrete frame-shear wall buildings using seismic isolation for resilient performance. *Structures*, 34, 4745–57, 2021. <https://doi.org/10.1016/j.istruc.2021.10.081>.
- [22] K. Jamdade, S. Dumne and P. Kalpana, Seismic analysis of multi-storied rcc building involving semi active vf damper and base isolators. *Journal of the Institution of Engineers (India): Series A*, 102, 1089–103, 2021. <https://doi.org/10.1007/s40030-021-00578-1>.
- [23] I. Imran, D. M. Siringoringo and J. Michael, Seismic performance of reinforced concrete buildings with double concave friction pendulum base isolation system: case study of design by Indonesian code. *Structures*, 34, 462–78, 2021. <https://doi.org/10.1016/j.istruc.2021.07.084>.
- [24] A. R. Özuygur and E. N. Farsangi, Influence of pulse-like near-fault ground motions on the base-isolated buildings with LRB devices. *Practice Periodical on Structural Design and Construction*, 26, 04021027, 2021. [https://doi.org/10.1061/\(ASCE\)SC.1943-5576.0000603](https://doi.org/10.1061/(ASCE)SC.1943-5576.0000603).
- [25] A. H. Deringöl and E. M. Güneyisi, Effect of using high damping rubber bearings for seismic isolation of the buildings. *International Journal of Steel Structures*, 21, 1698–722, 2022. <https://doi.org/10.1007/s13296-021-00530-w>.
- [26] A. Chinchole, C. Singh Tumrate and D. Mishra, Design of base isolation system for a six storey reinforced concrete building. *IOP Conference Series: Earth and Environmental Science*, 796, 012034, 2021. <https://doi.org/10.1088/1755-1315/796/1/012075>.
- [27] P. Clemente, A. D. Cicco, F. Saitta and A. Salvatori, Seismic behavior of base isolated civil protection operative center in Foligno, Italy. *Journal of Performance of Constructed Facilities*, 35, 04021027, 2021. [https://doi.org/10.1061/\(ASCE\)CF.1943-5509.0001589](https://doi.org/10.1061/(ASCE)CF.1943-5509.0001589).
- [28] N. Murota, S. Suzuki, T. Mori, K. Wakishima, B. Sadan, C. Tuzun, F. Sutcu and M. Erdik, Performance of high-damping rubber bearings for seismic isolation of residential buildings in Turkey. *Soil Dynamics and Earthquake Engineering*, 143, 106620, 2021. <https://doi.org/10.1016/j.soildyn.2021.106620>.
- [29] J. M. Jara, E. J. Hernández and B. A. Olmos, Effect of epicentral distance on the applicability of base isolation and energy dissipation systems to improve seismic behavior of RC buildings. *Engineering Structures*, 230, 111727, 2021. <https://doi.org/10.1016/j.engstruct.2020.111727>.
- [30] F. Micozzi, A. Flora, L. R. S. Viggiani, D. Cardone, L. Ragni and A. Dall’asta, Risk assessment of reinforced concrete buildings with rubber isolation systems designed by the Italian Seismic Code. *Journal of Earthquake Engineering*, 26 (14), 7245–75, 2021. <https://doi.org/10.1080/13632469.2021.1961937>.
- [31] A. Chanda and R. Debbarma, Probabilistic seismic analysis of base isolated buildings considering near and far field earthquake ground motions. *Structure and Infrastructure Engineering*, 18, 97–108, 2021. <https://doi.org/10.1080/15732479.2020.1836000>.
- [32] I. Gołębiewska and M. Dutkiewicz, Application of friction pendulum bearings in multistory buildings. *Acoustics and Vibration of Mechanical Structures-AVMS 2019, Part of the Springer Proceedings in Physics book series (SPPHY)*, 251, 453–61, 2021.
- [33] P. Sunagar, A. Bhashyam, M. Shashikant, K. S. Sreekeshava and A. K. Chaurasiya, Effect of different base isolation techniques in multistoried rc regular and irregular building. *Trends in Civil Engineering and Challenges for Sustainability, Part of the Lecture Notes in Civil Engineering book series (LNCE)* 99, 391–403, 2021.
- [34] S. Etedali, K. Hasankhoie and M. R. Sohrabi, Seismic responses and energy dissipation of pure-friction and resilient-friction base-isolated structures: A parametric study. *Journal of Building Engineering*, 29, 101194, 2020. <https://doi.org/10.1016/j.jobe.2020.101194>.
- [35] K. Ye, Y. Xiao and L. Hu, A direct displacement-based design procedure for base-isolated building structures with lead rubber bearings (LRBs). *Engineering Structures*, 197, 109402, 2019. <https://doi.org/10.1016/j.engstruct.2019.109402>.
- [36] H. Gazi and C. Alhan, Reliability of elastomeric-isolated buildings under historical earthquakes with/without forward-directivity effects. *Engineering*

- Structures, 195, 490–507, 2019. <https://doi.org/10.1016/j.engstruct.2019.05.081>.
- [37] S. Kitayama and M. C. Constantinou, Probabilistic seismic performance assessment of seismically isolated buildings designed by the procedures of ASCE/SEI 7 and other enhanced criteria. *Engineering Structures*, 179, 566–82, 2019. <https://doi.org/10.1016/j.engstruct.2018.11.014>.
- [38] C. Giarlelis, D. Koufalis and C. Repapis, Seismic isolation: An effective technique for the seismic retrofitting of a reinforced concrete building. *Structural Engineering International*, 30, 43–52, 2020. <https://doi.org/10.1080/10168664.2019.1678449>.
- [39] A. H. Deringöl and E. M. Güneyisi, Effect of friction pendulum bearing properties on behaviour of buildings subjected to seismic loads. *Soil Dynamics and Earthquake Engineering*, 125, 105746, 2019. <https://doi.org/10.1016/j.soildyn.2019.105746>.
- [40] F. Mazza, M. Mazza and Vulcano A, Base-isolation systems for the seismic retrofitting of r.c. framed buildings with soft-storey subjected to near-fault earthquakes. *Soil Dynamics and Earthquake Engineering*, 109, 209–21, 2018. <https://doi.org/10.1016/j.soildyn.2018.02.025>.
- [41] S. Kitayama and M. C. Constantinou, Collapse performance of seismically isolated buildings designed by the procedures of ASCE/SEI 7. *Engineering Structures*, 164, 243–58, 2018. <https://doi.org/10.1016/j.engstruct.2018.03.008>.
- [42] M. M. Nasery, M. Ergun, S. Ates and M. Husem, “Comparing the dynamic behavior of a hospital-type structure with fixed and isolated base. *Earthquakes and Structures*, 9, 657–71, 2015. <https://doi.org/10.12989/eas.2015.9.3.657>.
- [43] S. Ates S and M. Yurdakul, Site-response effects on RC buildings isolated by triple concave friction pendulum bearings. *Computers and Concrete*, 8, 693–715, 2011. <https://doi.org/10.12989/cac.2011.8.6.693>.
- [44] M. Yurdakul and S. Ates, Modeling of triple concave friction pendulum bearings for seismic isolation of buildings. *Structural Engineering and Mechanics*, 40, 315–34, 2011. <https://doi.org/10.12989/sem.2011.40.3.315>.
- [45] R. C. Ümütlü, H. Ozturk and B. Bidikli, A robust adaptive control design for active tuned mass damper systems of multistory buildings. *Journal of Vibration and Control*, 27, 2765–77, 2020. <https://doi.org/10.1177/1077546320966>.
- [46] M. Soleymani, A. H. Abolmasoumi, H. Bahrami, A. Khalatbari, E. Khoshbin and S. Sayahi, Modified sliding mode control of a seismic active mass damper system considering model uncertainties and input time delay. *Journal of Vibration and Control*, 24, 1051–64, 2016. <https://doi.org/10.1177/107754631665747>.
- [47] C. Collette and S. Chesné, Robust hybrid mass damper. *Journal of Sound and Vibration*, 375, 19–27, 2016. <https://doi.org/10.1016/j.jsv.2016.04.030>.
- [48] N. Mamat, F. Yakub, S. A. Z. Shaikh Salim and M. S. Mat Ali, Seismic vibration suppression of a building with an adaptive nonsingular terminal sliding mode control. *Journal of Vibration and Control*, 26, 2136–47, 2020. <https://doi.org/10.1177/10775463209153>.
- [49] R. Guclu and H. Yazici, Vibration control of a structure with ATMD against earthquake using fuzzy logic controllers. *Journal of Sound and Vibration*, 318, 36–49, 2008. <https://doi.org/10.1016/j.jsv.2008.03.058>.
- [50] L. Xu, Y. Cui and Z. Wang, Active tuned mass damper based vibration control for seismic excited adjacent buildings under actuator saturation. *Soil Dynamics and Earthquake Engineering*, 135, 106181, 2020. <https://doi.org/10.1016/j.soildyn.2020.106181>.
- [51] A. Hossein HEIDARI, S. Etedali, M. Reza JAVAHERI-TAFTI. A hybrid LQR-PID control design for seismic control of buildings equipped with ATMD. *Frontiers of Structural and Civil Engineering*, 12, 44–57, 2017. <https://doi.org/10.1007/s11709-016-0382-6>.
- [52] K. Karami, S. Manie, K. Ghafouri and S. Nagarajaiah, Nonlinear structural control using integrated DDA/ISMP and semi-active tuned mass damper. *Engineering Structures*, 181, 589–604, 2019. <https://doi.org/10.1016/j.engstruct.2018.12.059>.
- [53] UBC, Uniform Building Code, 1997.
- [54] TEBC-2018, General Directorate for Foundations, Turkey Earthquake Building Code, Ankara, Turkey, 2018.
- [55] General Directorate of Mineral Research and Exploration, MTA 2018. <http://www.mta.gov.tr/v3.0/>, Accessed 1 October 2022.
- [56] Disaster & Emergency Management Authority Presidential of Earthquake Department, AFAD. <https://depem.afad.gov.tr/>, Accessed 1 October 2022.
- [57] SAP2000, Integrated Finite Elements Analysis and Design of Structures, Computers and Structures, Inc., Berkeley, CA, USA 2019.
- [58] ANSYS, Swanson Analysis System, USA 2015.

